Acta Pharmaceutica Sinica B 2024;14(4):1726−1741

Chinese Pharmaceutical Association
Institute of Materia Medica, Chinese Academy of Medical Sciences

Acta Pharmaceutica Sinica B

www.elsevier.com/locate/apsb
www.sciencedirect.com

ORIGINAL ARTICLE

Endothelial phosphodiesterase 4B inactivation ameliorates endothelial-to-mesenchymal transition and pulmonary hypertension

Yanjiang Xing[a,c,†], Yangfeng Hou[a,†], Tianfei Fan[a,e,†], Ran Gao[a,†], Xiaohang Feng[a], Bolun Li[a], Junling Pang[a], Wenjun Guo[a], Ting Shu[a,c], Jinqiu Li[a], Jie Yang[a], Qilong Mao[a], Ya Luo[a], Xianmei Qi[a], Peiran Yang[a], Chaoyang Liang[b], Hongmei Zhao[d,*], Wenhui Chen[b,*], Jing Wang[a,c,*], Chen Wang[a]

[a]*State Key Laboratory of Respiratory Health and Multimorbidity, Institute of Basic Medical Sciences, Chinese Academy of Medical Sciences, Peking Union Medical College, Beijing 100005, China*
[b]*Department of Lung Transplantation, National Center for Respiratory Medicine, National Clinical Research Center for Respiratory Diseases, China−Japan Friendship Hospital, Institute of Respiratory Medicine, Chinese Academy of Medical Sciences, Beijing 100029, China*
[c]*Haihe Laboratory of Cell Ecosystem, Chinese Academy of Medical Sciences and Peking Union Medical College, Tianjin 300051, China*
[d]*The State Key Laboratory of Complex, Severe, and Rare Diseases, Institute of Basic Medical Sciences, Chinese Academy of Medical Sciences, Department of Pathophysiology, Peking Union Medical College, Beijing 100005, China*
[e]*Department of Pharmacy, West China Hospital, Sichuan University, Chengdu 610044, China*

Received 9 August 2023; received in revised form 13 December 2023; accepted 5 January 2024

KEY WORDS

Phosphodiesterase 4B;
Pulmonary hypertension;
Endothelial-to-mesenchymal transition;

Abstract Pulmonary hypertension (PH) is a fatal disorder characterized by pulmonary vascular remodeling and obstruction. The phosphodiesterase 4 (PDE4) family hydrolyzes cyclic AMP (cAMP) and is comprised of four subtypes (PDE4A−D). Previous studies have shown the beneficial effects of pan-PDE4 inhibitors in rodent PH; however, this class of drugs is associated with side effects owing to the broad inhibition of all four PDE4 isozymes. Here, we demonstrate that PDE4B is the predominant PDE isozyme in lungs and that it was upregulated in rodent and human PH lung tissues. We also confirmed that PDE4B

*Corresponding authors.
E-mail addresses: wangjing@ibms.pumc.edu.cn (Jing Wang), wenhuichen1004@sina.com (Wenhui Chen), hongmeizhao@ibms.pumc.edu.cn (Hongmei Zhao).
[†]These authors made equal contributions to this work.
Peer review under the responsibility of Chinese Pharmaceutical Association and Institute of Materia Medica, Chinese Academy of Medical Sciences.

https://doi.org/10.1016/j.apsb.2024.01.012

Protein kinase A;
Bone morphogenetic protein receptor II;
Side effects;
Lineage tracing;
Vascular remodeling

is mainly expressed in the lung endothelial cells (ECs). Evaluation of PH in *Pde4b* wild type and knockout mice confirmed that *Pde4b* is important for the vascular remodeling associated with PH. *In vivo* EC lineage tracing demonstrated that *Pde4b* induces PH development by driving endothelial-to-mesenchymal transition (EndMT), and mechanistic studies showed that *Pde4b* regulates EndMT by antagonizing the cAMP-dependent PKA−CREB−BMPRII axis. Finally, treating PH rats with a PDE4B-specific inhibitor validated that PDE4B inhibition has a significant pharmacological effect in the alleviation of PH. Collectively, our findings indicate a critical role for PDE4B in EndMT and PH, prompting further studies of PDE4B-specific inhibitors as a therapeutic strategy for PH.

1. Introduction

Pulmonary hypertension (PH) is a progressive disease characterized by increased pulmonary vascular resistance and persistently elevated pulmonary arterial pressure, ultimately leading to right heart failure and death[1]. PH is associated with pulmonary vascular remodeling, which causes pulmonary vascular obstruction and stiffness. Most treatments currently prescribed for patients with PH rely on reducing vascular resistance by stimulating pulmonary vascular dilation in pulmonary smooth muscle cells. However, what is urgently needed are therapeutic strategies to alleviate or delay vascular remodeling.

Cyclic adenosine monophosphate (cAMP) and cyclic guanosine monophosphate (cGMP) act as second messengers in a variety of signaling pathways involved in cardiovascular diseases[2]. Regarding PH, cAMP and cGMP signaling are downstream of nitric oxide and PGI_2, and impaired cAMP and cGMP signaling is a hallmark of PH[3]. Phosphodiesterases (PDEs) are a superfamily of enzymes that hydrolyze cAMP and/or cGMP, and the 11 families of PDEs (PDE1−PDE11)[4] are characterized by differences in enzymatic properties, regulatory control, and cellular/subcellular expression. Thus, the different PDE families modulate distinct cyclic nucleotide signaling molecules and elicit different biological responses[5].

PDE4 and PDE5, which hydrolyze cAMP and cGMP[6], respectively, are the main PDEs in lung tissues[7,8]. PDE5 inhibitors, such as sildenafil and tadalafil, are used clinically to treat PH. On the other hand, pan-PDE4 inhibitors, such as roflumilast, are prescribed for the treatment of several inflammatory diseases, including chronic obstructive pulmonary disease (COPD), asthma, psoriasis, and atopic dermatitis[9−13]. Although studies have shown that roflumilast attenuates PH in rats[14,15], it is not currently used in the treatment of PH. This is owing to, in part, side effects associated with pan-PDE4 inhibitors that make them poorly tolerated, such as nausea and vomiting. The PDE4 family is encoded by four different genes, *PDE4A, PDE4B, PDE4C,* and *PDE4D,* and the encoded isozymes have distinct tissue/cell expression patterns and functional roles. Their broad functions and distribution are likely to contribute to the side effects associated with pan-PDE4 inhibitor drugs; for example, the emetic side effects of pan-PDE4 inhibitors have been linked to PDE4D expression in the nervous system[16,17]. Therefore, identifying the PDE4 isozyme(s) that are most biologically relevant to the pathology of PH could guide the development of PDE4 isozyme-specific inhibitors.

In this study, we identified PDE4B as a driver of PH development. We found that PDE4B expression was profoundly upregulated in lung tissues from patients with PH as well as in rodent models of PH. Treatment of a *Pde4b*-knockout mouse model of PH with roflumilast demonstrated that *Pde4b* is the primary target through which roflumilast impacts PH development. Further, we determined that PDE4B expression in the lung is primarily within the endothelial cells (ECs). Using *Pde4b*-knockout mice engineered to enable EC-specific lineage tracing, we showed that *Pde4b* is required for endothelial-to-mesenchymal transition (EndMT), which contributes to PH development. Mechanistically, we determined that *Pde4b* regulates EndMT by antagonizing signaling through the protein kinase A-cAMP-response element binding protein-bone morphogenetic protein receptor II (PKA−CREB−BMPRII) axis. More directly, treating PH rats with newly discovered PDE4B-specific inhibitor validated that PDE4B inhibition can exert a significant therapeutical effect on the PH. Our findings identify a specific PDE isozyme, PDE4B, as a driver of PH development that induces PH-related vascular remodeling. These data suggest that development of inhibitor drugs targeting PDE4B may effectively treat patients with PH by alleviating vascular remodeling and potentially with improved tolerability compared to pan-PDE4 inhibitors.

2. Materials and methods

2.1. Human lung collection

Human specimens were obtained from patients who gave informed consent under protocols approved by the Institutional Committee of Peking Union Medical College (Project Number: 2018043) and the China−Japan Friendship Hospital Lung Transplantation Center (Project Number: 2019-164-K113). Human pulmonary hypertension (PH) lung tissues were obtained from patients with PH who received lung transplantation. The diagnosis of PH was based on the 2015 ESC/ERS guidelines[18]. Specimens from patients with lung infection, autoimmune diseases and complicated pulmonary disease (tumor, fibrosis, etc.) were excluded. Non-PH lung tissues were collected from donors during lung transplantation. Lung tissues were immediately fixed in 10% formaldehyde and embedded in paraffin for histological analysis, or frozen at −80 °C for further use after surgery or dissection. The investigation conformed to the principles outlined in the Declar

ation of Helsinki. Clinical information associated with the samples is shown in Supporting Information Table S1.

2.2. Animal models

Pde4b^{WT} mice (C57BL/6 J) were obtained from The Jackson Laboratory. *Pde4b*^{KO} mice, *Pde4b*$^{flox/flox}$, and Tek-Cre mice were generated and obtained by Shanghai Model Organisms Center, Inc. using CRISPR/Cas9 technology. Double-transgenic mice with endothelial genetic lineage markings were generated by crossing Tek-Cre mice with mTomato/mGFP-floxed dual-fluorescent Cre reporter mice (mTmG mice) (Shanghai Model Organisms Center, Inc.). Sprague−Dawley (SD) rats were provided by the Beijing HFK Bioscience. The researchers were blinded to animal genotype and grouping information.

The animals were randomized into different experimental groups. All animal experiments conformed to the Guide for the Care and Use of Laboratory Animals published by the US National Institutes of Health and were approved by the Animal Care and Use Committee of Peking Union Medical College (Accreditation Number: ACUC-A01-2017-007). Additional details are described in Supporting Information.

2.3. Echocardiography

Echocardiography was performed using the Vevo 2100 High-Resolution Imaging System (FUJIFILM VisualSonics) equipped with a 30-MHz scan head, as described[19,20]. Mice or rats were anesthetized with isoflurane inhalation using a vaporizer at 0.5%−1.5% and placed on the homeothermic plate in supine position after thoracic and abdominal depilation. Transthoracic echocardiography from the parasternal short axis view at the aortic valve level was performed to measure pulmonary artery acceleration time (PA AT) and pulmonary artery ejection time (PA ET).

2.4. Hemodynamic measurement

For mice, the right ventricular systolic pressure (RVSP) was measured directly by closed-chest right ventricular puncture as described[21,22]. The mice were anesthetized with pentobarbital sodium (50 mg/kg, intraperitoneally). Heparin sodium (10 mg/mL) was infused into the intravenous infusion needle and the three-way pipe connected to a pressure transducer (Xinhangxingye). After incision of the skin starting from the sternum and extending to the ribs, the intravenous needle was inserted into the right ventricle from the infrastructural angle.

For rats, the RVSP was measured by a pulmonary embolism catheter which inserted through the right jugular vein into the right ventricle as described[23]. The rats were anesthetized with 12% urethane (1.2 g/kg, intraperitoneally). Heparin sodium (10 mg/mL) was infused into the catheter and the three-way pipe connected to the pressure transducer.

RVSP was transmitted to the Bridge Amp (AD Instruments) through the pressure transducer. Data were collected and analysed using the PowerLab data acquisition system (AD Instruments) and LabChart 7.2 software (AD Instruments).

2.5. Histological analysis

After measuring RVSP, the pulmonary circulation was flushed with phosphate buffered saline (PBS) from the right ventricle, then the heart and lungs were removed. The right ventricle was carefully separated from the heart and weighed. Right ventricular hypertrophy was assessed by calculating the ratio of the weight of right ventricle (RV) to the weight of the left ventricle (LV) and septum (S) [RV/(LV + S)].

The left lungs were fixed for 24 h in 10% neutral formalin solution, and the right lungs were placed in liquid nitrogen for protein and RNA extraction. After paraffin embedding, the slides (6 μm thickness) were sectioned using Leica RM2255 Fully Automated Rotary Microtome (Leica) and were stained for morphological analysis.

H&E and immunohistochemical staining was performed according to the manufacturer's instructions. Additional details are described in Supporting Information.

2.6. Cell culture, siRNA treatment and lentiviral transfection

Mouse pulmonary artery endothelial cells (PAECs) were purchased from American Type Culture Collection and cultured in ECM (ScienCell) containing 5% fetal bovine serum, 100 U/mL penicillin, and 100 g/mL streptomycin. PAECs between passage 5 to 12 were used in all experiments. To simulate the pathological state of PH *in vitro*, PAECs were cultured in 6-well plates and were placed in a hermetic cell incubator containing 1% oxygen concentration for 24 h before harvest. To knockdown or overexpress *Pde4b* in PAECs, siRNA treatment and lentiviral transfection were performed respectively. Additional details are described in Supporting Information.

2.7. Immunofluorescence analysis

Paraffin sections were deparaffinized and rehydrated before antigen retrieval as described above. PAECs were fixed with 4% paraformaldehyde for 15 min. Images were photographed using NIKON DS-Ri2 Microscope Digital Camera System (NIKON). We obtained similar results from at least 3 independent experiments. Additional details are described in Supporting Information.

2.8. Western blot analysis

Protein was extracted from lung tissues or PAECs in lysis buffer according to the manufacturer's instructions. Protein expression was measured by analyzing the intensities of the protein bands with Image-Pro Plus 6.0 software. Additional details are described in Supporting Information.

2.9. Real-time polymerase chain reaction (RT-PCR)

Total RNA was extracted from lung tissues or PAECs using TRIzol Reagent (Invitrogen) according to the manufacturer's protocol. Target gene mRNA expression fold change compared with control group was calculated using the $2^{-\Delta\Delta Ct}$ method. Additional details are described in Supporting Information. The RT-PCR primers are shown in Supporting Information Table S2.

2.10. Cell counting kit-8 (CCK8) assay

The proliferation of PAECs with different treatments was determined using the CCK-8 Assay Kit (Beyotime, Cat#: C0038) according to the manufacturer's instructions and previous studies[21,24]. Cell proliferation was detected using BioTek Synergy HTX Multimode Reader (BioTek Instrument, Inc.) to measure

absorbance at 450 nm. Additional details are described in Supporting Information.

2.11. 5-Ethynyl-2′-deoxyuridine (EdU) labeling assay

PAEC proliferation was also detected using an EdU Cell Proliferation Kit (Beyotime) according to the manufacturer's instructions and previous studies[21,25]. The degree of proliferation was expressed as the proportion of EdU-positive cells in total cells from 3 random fields for each individual experiment. Additional details are described in Supporting Information.

2.12. Scratch wound assay

The migration of PAECs with different treatments was detected *via* scratch wound assay according to previous studies[26,27]. The degree of cell migration was expressed by wound closure, which was the proportion of reduced area size post-wounding relative to the original area size from 3 random fields for each individual experiment. Additional details are described in Supporting Information.

2.13. Transwell migration assay

PAEC migration was evaluated *via* Transwell migration assay according to the manufacturer's instructions and previous studies[26,28]. The degree of migration was quantified by the number of cells migrating through the pore filters from 3 random fields for each individual experiment. Additional details are described in Supporting Information.

2.14. Statistical analysis

All *in vitro* experiments were performed independently at least three times. Data were analyzed using GraphPad Prism 9 (GraphPad Software Inc.). Shapiro−Wilk test was used to test for normal distribution. Brown−Forsythe test or F test was used to test for equality of variances. Normally distributed data with equal variance was analyzed using the parametric unpaired Student's *t* test for 2 independent groups and the parametric one-way ANOVA or two-way ANOVA followed by the Holm-Sidak's *post hoc* test for experiments with $\geq$3 groups. Normally distributed data with reject equal variance were analyzed using parametric Welch's *t* test for 2 independent groups and the parametric Welch ANOVA with Dunnett's T3 *post hoc* test for experiments with $\geq$3 groups. Where a normal distribution could not be confirmed, the nonparametric Mann−Whitney test was used for 2 independent groups or nonparametric ANOVA Kruskal−Wallis test with post Dunn's multiple comparisons test was used for experiments with $\geq$3 groups. Data are expressed as mean $\pm$ standard error of the mean (SEM) for normally distributed datasets, and data are expressed as median $\pm$ interquartile range for nonnormally distributed datasets. $P < 0.05$ is considered statistically significant. $^{*}P < 0.05$, $^{**}P < 0.01$, $^{***}P < 0.001$, $^{****}P < 0.0001$.

3. Results

3.1. PDE4B expression is upregulated in PH patients and animal models

To characterize the expression profile of PDE4 isozymes in lung tissues, we measured the mRNA levels of *Pde4a, Pde4b, Pde4c* and *Pde4d* in lung tissues from the SU5416/hypoxia (SuHx)-induced PH mouse model. We found that *Pde4b* was the most highly expressed in the lungs of non-induced animals (normoxia), and that its expression was significantly upregulated in lung tissue after SuHx induction to establish PH. No significant changes in expression were observed between non-induced and induced lung tissues for *Pde4a*, *Pde4c* and *Pde4d* (Fig. 1A). Similar results were observed in a hypoxia-induced PH mouse model (Fig. 1B) as well as in monocrotaline (MCT)-induced and SuHx-induced rat models of PH (Fig. 1C and D). Consistent with our rodent data, in human lung samples (Table S1), *PDE4B* was the most highly expressed PDE4 isozyme in normal lung tissue, and *PDE4B* was robustly upregulated in tissue from patients with PH (Fig. 1E). Western blot analysis confirmed that the PDE4B protein was also upregulated in pathological lung tissues in all of the rodent models as well as in the PH tissue samples from patients (Fig. 1F and J). These results indicate that PDE4B may be associated with PH development, and it was prioritized for further characterization.

3.2. Pde4b knockout attenuates PH development

To investigate the role of PDE4B in PH development, we generated global *Pde4b* knockout mice ($Pde4b^{KO}$) and confirmed loss of PDE4B protein in lung tissues (Supporting Information Fig. S1A−S1C). PH was established by SuHx induction for 3 weeks in 8-week-old mice (Fig. 2A). Compared to SuHx-induced wild type mice ($Pde4b^{WT}$), SuHx-induced $Pde4b^{KO}$ mice exhibited lower right ventricular systolic pressure (RVSP) (Fig. 2B) as well as a reduced ratio of right ventricle (RV) to left ventricle (LV) plus septum (S) weight [RV/(LV + S)] (Fig. 2C), indicating that $Pde4b^{KO}$ mice had improved ventricular hypertrophy. The pulmonary artery acceleration time/ejection time (PA AT/ET) ratio was also attenuated in $Pde4b^{KO}$ mice compared to $Pde4b^{WT}$ mice, suggesting *Pde4b* loss reduced pulmonary artery back-pressure and could potentially restore diastolic function (Fig. 2D). In addition, hematoxylin and eosin (H&E) and α-SMA immunostaining revealed that the medial wall thickness of distal pulmonary arteries with diameter $<$100 μm was reduced in $Pde4b^{KO}$ mice compared to $Pde4b^{WT}$ mice (Fig. 2E−H). Together, these data strongly indicate that PDE4B plays an important role in the detrimental vascular remodeling associated with PH.

3.3. Roflumilast inhibits PDE4B and attenuates the SuHx-induced PH phenotype

The pan-PDE4 inhibitor roflumilast has been used in clinical treatment of COPD, and it has also been shown to attenuate PH development in rat models[14,15]. We therefore examined the therapeutic effect of roflumilast in mice with established PH. $Pde4b^{WT}$ mice at 8 weeks of age were subjected to SuHx for 3 weeks to establish PH, and then mice were randomized to receive the pan-PDE4 inhibitor roflumilast (2 mg/kg·day) or vehicle control by oral gavage for an additional 2 weeks (Supporting Information Fig. S2A). We observed that RVSP was reduced in the SuHx-induced mice treated with roflumilast compared with the SuHx-induced mice treated with vehicle (Fig. S2B). Roflumilast treatment also significantly decreased the ratio of RV/(LV + S) and improved PA AT/ET ratio (Fig. S2C and S2D). The average medial wall of distal pulmonary arteries was lower in SuHx-induced mice treated with roflumilast than in SuHx-induced mice treated with vehicle (Fig. S2E−S2H). Thus, our results further demonstrate that roflumilast has a significant pharmacological impact in the alleviation of PH in mice.

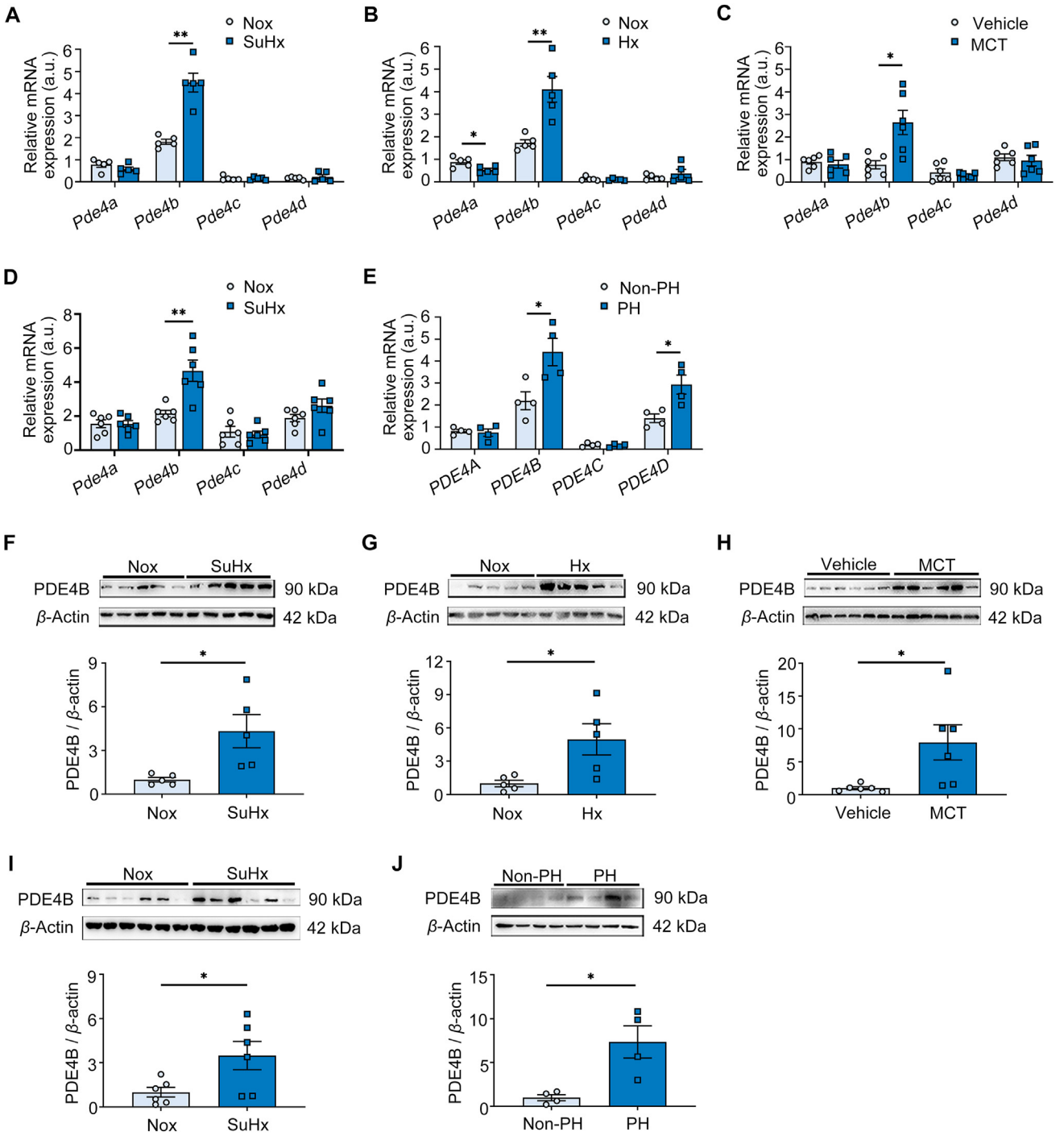

Figure 1 PH development changes PDE4 isoform expression. (A) Real-time polymerase chain reaction (RT-PCR) quantification of *Pde4a*, *Pde4b*, *Pde4c* and *Pde4d* mRNA levels (fold change normalized to controls) in lung tissues of control ($n = 5$) and SuHx-induced PH mice ($n = 5$). (B) RT-PCR quantification of *Pde4a*, *Pde4b*, *Pde4c* and *Pde4d* mRNA levels (fold change *versus* controls) in the lung tissues of control ($n = 5$) and hypoxia (Hx)-induced PH mice ($n = 5$). (C) RT-PCR quantification of *Pde4a*, *Pde4b*, *Pde4c* and *Pde4d* mRNA levels (fold change *versus* control) in the lung tissues of control ($n = 6$) and monocrotaline (MCT)-induced PH rats ($n = 6$). (D) RT-PCR quantification of *Pde4a*, *Pde4b*, *Pde4c* and *Pde4d* mRNA levels (fold change *versus* controls) in the lung tissues of control ($n = 6$) and SuHx-induced PH rats ($n = 6$). (E) RT-PCR quantification of *PDE4A*, *PDE4B*, *PDE4C* and *PDE4D* mRNA levels (fold change *versus* donor subjects) in the lung tissues from donors ($n = 4$) and patients with PH ($n = 4$). (F) Representative Western blots and quantification of PDE4B protein levels in lung tissues of control ($n = 5$) and SuHx-induced PH mice ($n = 5$), normalized to β-actin (fold change *versus* controls). (G) Representative Western blots and quantification of PDE4B protein levels in lung tissues of control ($n = 5$) and Hx-induced PH mice ($n = 5$), normalized to β-actin (fold change *versus* controls). (H) Representative Western blots and quantification of PDE4B protein levels in lung tissues of control ($n = 6$) and MCT-induced PH rats ($n = 6$), normalized to β-actin (fold change *versus* controls). (I) Representative Western blots and quantification of PDE4B protein levels in lung tissues of control ($n = 6$) and SuHx-induced PH rats ($n = 6$), normalized to β-actin (fold change *versus* controls). (J) Representative

To determine whether the effect of roflumilast on PH is the result of inhibiting PDE4B, we applied roflumilast to PH mice with or without *Pde4b* knockout (Fig. 2I). Interestingly, as shown by decreased RVSP and the ratio of RV/(LV + S) (Fig. 2J and K), increased PA AT/ET ratio (Fig. 2L), and reduced medial wall thickness of the distal pulmonary arteries (diameter <100 μm; Fig. 2M−P), the extent to which PH development was inhibited by roflumilast in $Pde4b^{WT}$ animals was similar to the inhibition observed in $Pde4b^{KO}$ animals, strongly implicating *Pde4b* as the major PDE4 isozyme through which roflumilast exerts its anti-PH effects.

3.4. *Pde4b deficiency in ECs alleviates SuHx-induced PH*

To study the underlying mechanism of PDE4B in PH development, we analyzed the single-cell sequencing data of lung tissues from control and SuHx-induced mice. Single-cell sequencing data showed that *Pde4b* is expressed most prominently in ECs, and is solely and significantly elevated in ECs during PH (Supporting Information Fig. S3A and S3B). Histological analysis of PDE4B and CD31 (an EC marker) expression confirmed that PDE4B was largely detected in the CD31-positive area (intima layer) of blood vessels in the lung tissues of PH patients (Fig. 3A) as well as in PH mouse models (Fig. 3B). Based on these finding, we evaluated *Pde4b* expression in mouse pulmonary artery endothelial cells (PAECs) under normoxic and hypoxic (1% O_2) conditions, which showed increased *Pde4b* mRNA (Fig. 3C) and protein (Fig. 3D) levels in PAECs grown in hypoxic conditions compared to normoxic conditions (Fig. 3C and D). As ECs play an essential role in vascular remodeling associated with PH[29], we hypothesized the PDE4B expressed in ECs may contribute to PH development.

To test our hypothesis, we engineered SuHx-induced PH mice with *Pde4b* knockout specifically in ECs ($Pde4b^{EC-/-}$). To accomplish this, we first generated mice in which exon 7 of *Pde4b* was floxed ($Pde4b^{flox/flox}$) to allow homologous recombination using CRISPR/Cas9 technology. We then crossed $Pde4b^{flox/flox}$ mice with Tek-Cre mice to obtain $Pde4b^{EC-/-}$ mice ($Pde4b^{flox/flox}$, Tek-$cre^{+/-}$) (Fig. S3C). $Pde4b^{flox/flox}$ mice were used as controls. Immunoblotting (Fig. S3D) and immunostaining (Fig. S3E) confirmed significant depletion of PDE4B in $Pde4b^{EC-/-}$ mice, particularly in ECs of lung tissues, compared to controls. Analysis of PH pathology in SuHx-induced mice revealed that RVSP was attenuated and the ratio of RV/(LV + S) was decreased in $Pde4b^{EC-/-}$ mice compared to $Pde4b^{flox/flox}$ mice (Fig. 3E−G). Consistently, compared to $Pde4b^{flox/flox}$ mice, PA AT/ET was mitigated and medial wall thickness of distal pulmonary arteries <100 μm in diameter was reduced in $Pde4b^{EC-/-}$ mice (Fig. 3H−L). These results indicate that PDE4B in ECs promotes pulmonary vascular remodeling and PH development. Notably, EC-specific *Pde4b* knockout improved PH parameters similarly to global *Pde4b* knockout, which suggests that PDE4B in ECs may be the major contributor to PH versus PDE4B in other cell types.

3.5. *Pde4b knockout in ECs prevents EndMT in vivo*

In injured vessels, ECs undergo a phenotypic transformation to mesenchymal cells, a process referred to as EndMT. During this process, endothelial cells lose endothelial characteristics, such as endothelial morphology and EC-specific gene expression, and gain mesenchymal characteristics. The mesenchymal phenotype has been shown to contribute to vascular remodeling and stiffness[30], and EndMT has been observed in lung tissues from patients with pulmonary arterial hypertension (PAH) and from experimental models of PH, including models induced by MCT or hypoxia combined with SU5416[31]. To determine whether PDE4B is involved in EndMT *in vivo* during PH development, we qualitatively assessed colocalization of CD31 and a mesenchymal marker, α-SMA, in lung tissue from a SuHx-induced mouse model (Fig. 4A). Colocalization of CD31 and α-SMA was significantly higher in SuHx-induced $Pde4b^{flox/flox}$ mice compared to normoxic controls (Fig. 4A), confirming that EndMT occurred in the SuHx-induced PH model. Importantly, colocalization of CD31 and α-SMA was reduced in SuHx-induced $Pde4b^{EC-/-}$ mice compared to SuHx-induced $Pde4b^{flox/flox}$ mice (Fig. 4A). Furthermore, mRNA and protein expression levels of endothelial markers (vWF, CD31, and VE-cadherin) were reduced, while expression levels of mesenchymal markers (α-SMA, Sm22α, and Vimentin) were increased in SuHx-induced $Pde4b^{flox/flox}$ mice compared to normoxic $Pde4b^{flox/flox}$ mice (Fig. 4B−N). Consistently, changes in EndMT markers were significantly attenuated in SuHx-induced $PDE4B^{EC-/-}$ mice compared to SuHx-induced $Pde4b^{flox/flox}$ mice (Fig. 4B−N). Similarly, EndMT was significantly reduced in SuHx-induced $Pde4b^{KO}$ mice compared to SuHx-induced $Pde4b^{WT}$ mice (Supporting Information Fig. S4), and the effects of global and EC-specific *Pde4b* knockout on attenuation of EndMT were similar (Fig. 4B−N, Fig. S4B−S4N). These results further support a dominant role of PDE4B in ECs in EndMT during PH development.

To further confirm the role of PDE4B in EndMT, we generated a mouse strain with combined EC-specific lineage tracing and *Pde4b* deficiency in ECs. We crossed Tek Cre/mTomato/mGreen (mTmG) mice with $Pde4b^{EC-/-}$ mice to obtain $Pde4b^{EC-/-}$/mTmG mice in which the EC lineages could be followed using the mGreen reporter (Fig. 4O). We then used Tek Cre/mTmG mice and $PDE4B^{EC-/-}$/mTmG mice to establish a SuHx-induced PH model. Similar to the $Pde4b^{EC-/-}$ mice, $Pde4b^{EC-/-}$/mTmG mice were protected from PH (Supporting Information Fig. S5A−S5H). To evaluate EndMT, we performed immunofluorescence staining of lung tissue to detect GFP and α-SMA, where GFP and α-SMA double-positive cells represented ECs undergoing EndMT. We found that ECs with EndMT markers were significantly increased in SuHx-induced Tek Cre/mTmG mice compared to uninduced controls, but were significantly reduced in SuHx-induced $Pde4b^{EC-/-}$/mTmG mice compared to SuHx-induced Tek Cre/mTmG mice (Fig. 4P). These data support that EndMT occurs during PH development and that PDE4B contributes to EndMT *in vivo*.

3.6. *PDE4B promotes hypoxia-induced EndMT in PAECs*

Next, we characterized the effects of *Pde4b* knockout in PAECs *in vitro*. Hypoxia-induced morphological changes from cobblestone-shaped to spindle-shaped cells were significantly

Western blots and quantification of PDE4B protein levels in lung tissues from donors ($n = 4$) and patients with PH ($n = 4$), normalized to β-actin (fold change *versus* controls). a.u.: arbitrary unit; Nox, Normoxia. Data are expressed as mean ± SEM. For (A) and (B), the differences between groups were determined using the Mann−Whitney test. For (C)−(E), the differences between groups were determined using unpaired Student's *t* test. For (F)−(J), the differences between groups were determined using parametric Welch's *t* test. *$P < 0.05$, **$P < 0.01$.

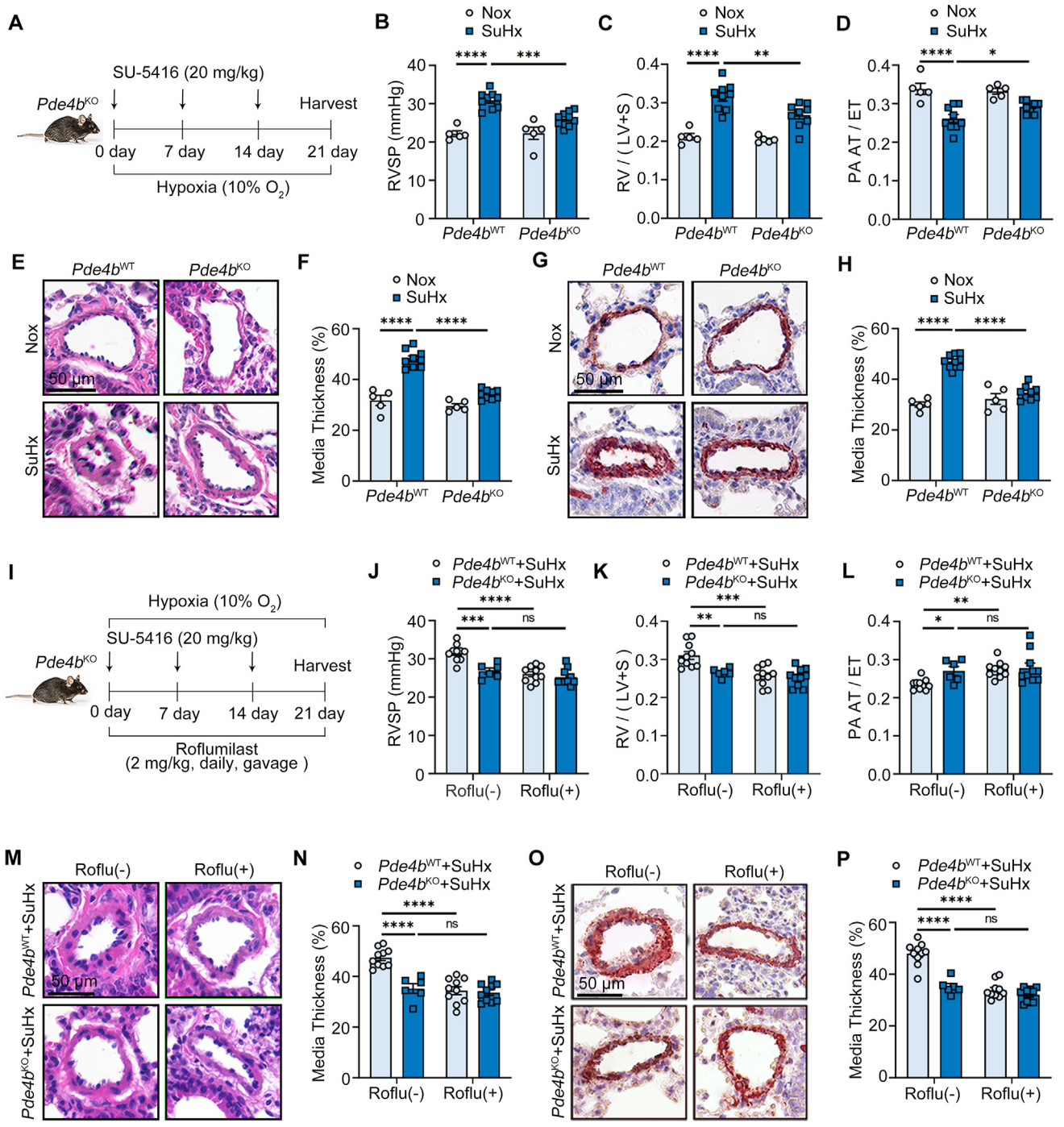

Figure 2 PDE4B is the most important isozyme driving PH development. (A) *Pde4b*^{WT} mice were subjected to Nox ($n = 5$) or SuHx ($n = 9$), and *Pde4b*^{KO} mice were subjected to Nox ($n = 5$) or SuHx ($n = 9$) for 3 weeks. (B)−(D) Right ventricular systolic pressure (RVSP) (B), left ventricle (LV) and septum (S) [RV/(LV + S)] (C), and cardiac echo analysis of pulmonary artery acceleration time/ejection time (PA AT/ET) ratio (D) in *Pde4b*^{WT} or *Pde4b*^{KO} mice subjected to Nox or SuHx in (A). (E) Representative hematoxylin and eosin (H&E) staining images of pulmonary arteries under the indicated experimental conditions; scale bar = 50 μm. (F) Pulmonary arterial wall thickness of mice in (E). (G) Representative images showing immunostaining of α-SMA in lung tissues; scale bar = 50 μm. (H) Pulmonary arterial wall thickness of mice in (G). (I) *Pde4b*^{WT} or *Pde4b*^{KO} mice subjected to SuHx were treated with vehicle or 2 mg/kg·day roflumilast (Roflu) by oral gavage for 3 weeks. *Pde4b*^{WT} SuHx mice treated with vehicle ($n = 10$) or Roflu ($n = 10$); *Pde4b*^{KO} SuHx mice treated with vehicle ($n = 6$) or Roflu ($n = 10$). (J)−(L) RVSP (J), ratio of RV/(LV + S) (K), cardiac echo analysis of PA AT/ET ratio (L) of indicated groups of mice in (I). (M) Representative H&E staining images of pulmonary arteries under the indicated experimental conditions; scale bar = 50 μm. (N) Pulmonary arterial wall thickness of mice in (M). (O) Representative immunostaining of α-SMA in lung tissues; scale bar = 50 μm. (P) Pulmonary arterial wall thickness of mice in (O). Data are expressed as mean ± SEM. For (B)−(D), (F), (H), (J)−(K), (N), (P), the differences between groups were determined using two-way ANOVA followed by the Holm-Sidak's *post hoc* test. For (L), the differences between groups were determined using nonparametric ANOVA Kruskal−Wallis test with post Dunn's multiple comparisons test. *$P < 0.05$, **$P < 0.01$, ***$P < 0.001$, ****$P < 0.0001$. ns, no significance.

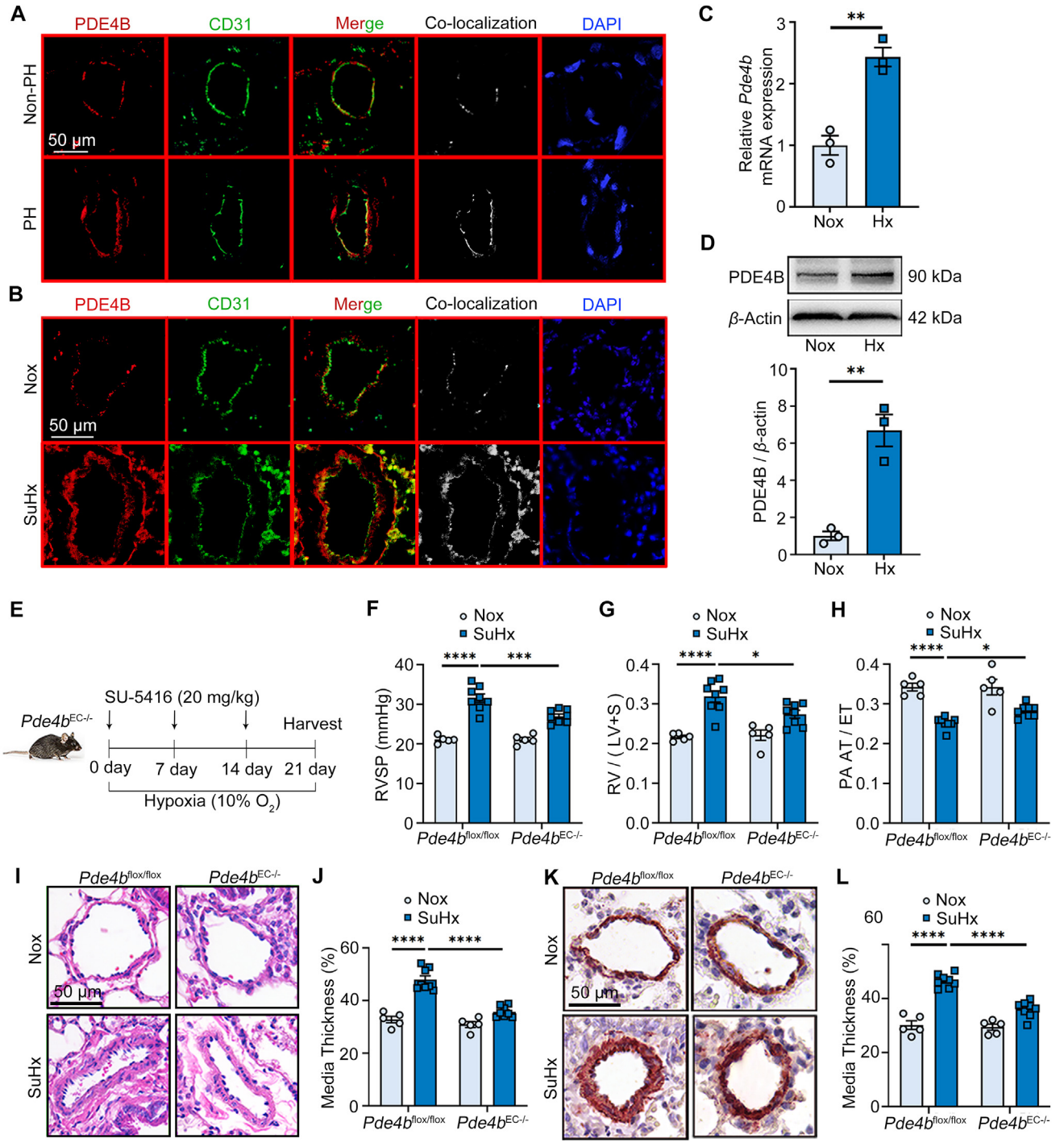

Figure 3 *Pde4b* knockout in ECs alleviates SuHx-induced PH. (A) Representative immunofluorescence staining of PDE4B and CD31 in lung tissues from donors and patients with PH; scale bar = 50 μm. (B) Representative immunofluorescence staining of PDE4B and CD31 in lung tissues of control and SuHx-induced PH mice; scale bar = 50 μm. Similar results were obtained from at least 3 independent experiments in (A) and (B). (C) RT-PCR analysis of *Pde4b* expression in mouse PAECs exposed to hypoxia (Hx). (D) Representative Western blots and quantification of PDE4B protein levels in PAECs exposed to Hx normalized to β-actin protein (fold change *versus* control). (E) $Pde4b^{flox/flox}$ or $Pde4b^{EC-/-}$ mice were subjected to normoxia (Nox) or SuHx for 3 weeks. $Pde4b^{flox/flox}$ mice subjected to Nox ($n = 5$) or SuHx ($n = 8$); $Pde4b^{EC-/-}$ mice subjected to Nox ($n = 5$) or SuHx ($n = 8$). (F)−(H) RVSP (F), ratio of RV/(LV + S) (G), and cardiac echo analysis of PA AT/ET ratio (H) in $Pde4b^{flox/flox}$ or $Pde4b^{EC-/-}$ mice subjected to Nox or SuHx in (E). (I) Representative H&E staining images of pulmonary arteries under indicated experimental conditions; scale bar = 50 μm. (J) Pulmonary arterial wall thickness of mice in (I). (K) Representative images showing immunohistochemistry staining of α-SMA in lung tissues; scale bar = 50 μm. (L) Pulmonary arterial wall thickness of mice in (K). Data are expressed as mean ± SEM. For (C) and (D), the differences between groups were determined using unpaired Student's *t* test. For (F)−(H), (J), (L), the differences between groups were determined using two-way ANOVA followed by the Holm-Sidak's *post hoc* test. $^{*}P < 0.05$, $^{**}P < 0.01$, $^{***}P < 0.001$, $^{****}P < 0.0001$.

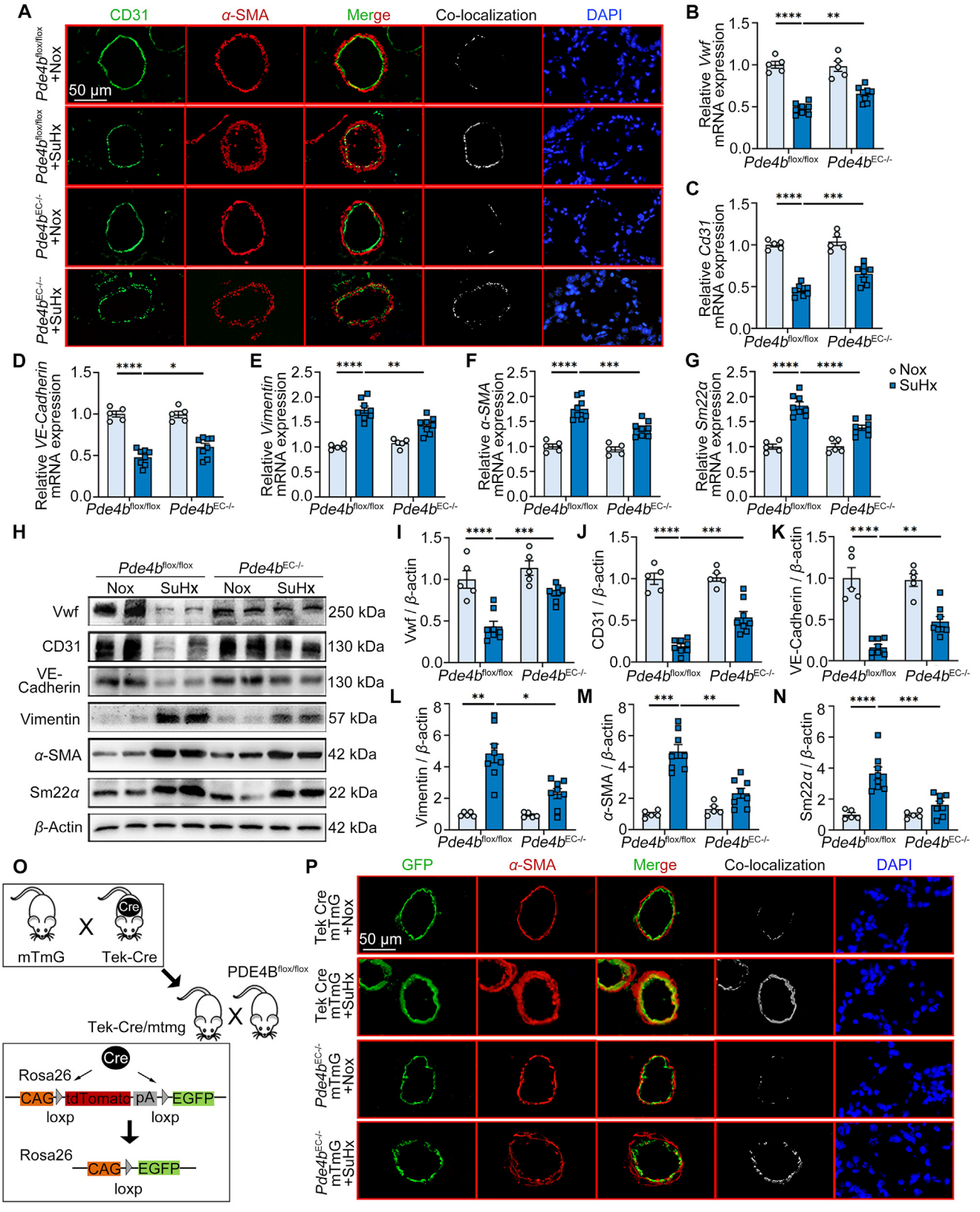

Figure 4 *Pde4b* knockout prevents EndMT in PH *in vivo*. (A) Representative immunofluorescence staining of CD31 and α-SMA in lung tissues of *Pde4b*$^{flox/flox}$ or *Pde4b*$^{EC-/-}$ mice subjected to normoxia (Nox) or SuHx; scale bar = 50 μm. Similar results were obtained from at least 3 independent experiments. (B)−(G) RT-PCR analysis of *Vwf* (B), *Cd31* (C), *VE-Cadherin* (D), *Vimentin* (E), *α-SMA* (F) and Smooth muscle 22α (*Sm22α*) (G) mRNA expression in *Pde4b*$^{flox/flox}$ or *Pde4b*$^{EC-/-}$ mice subjected to Nox or SuHx. (H) Representative immunoblot analysis of endothelial markers (Vwf; CD31; VE-Cadherin) and mesenchymal markers (Vimentin; α-SMA; Sm22α) in *Pde4b*$^{flox/flox}$ or *Pde4b*$^{EC-/-}$ mice

reversed in *Pde4b*-knockdown PAECs compared to controls (Supporting Information Fig. S6A−S6C, Fig. 5A). Immunofluorescence staining showed similar increases in colocalization of CD31 and α-SMA in PAECs that were either cultured in hypoxic conditions or treated with transforming growth factor TGF-β1, a well-known stimulator of EndMT[32], compared to cells cultured in normoxia or not and treated with TGF-β1, respectively (Fig. 5B, Fig. S6D and S6E). Consistent with our other results, the colocalization of EndMT markers induced by hypoxia was abrogated in *Pde4b*-knockdown PAECs (Fig. 5B). Also, mRNA and protein levels of endothelial markers (Vwf, CD31, VE-Cadherin) were higher and mRNA and protein levels of mesenchymal markers (Vimentin, α-SMA, Sm22α) were lower in *Pde4b*-knockdown PAECs compared to controls (Fig. 5C−G, Supporting Information Fig. S8A−S8I). These results suggest that *Pde4b* knockdown decreased EndMT in PAECs.

Moreover, we also detected the effects of *Pde4b* overexpression in PAEC EndMT *in vitro*. The results showed that hypoxia-induced spindle-shaped changes of PAECs were aggravated when *Pde4b* was overexpressed in ECs (Supporting Information Fig. S7, Fig. 5H). And the colocalization of EndMT markers induced by hypoxia was increased in *Pde4b*-overexpressed PAECs (Fig. 5I). Furthermore, mRNA and protein levels of endothelial markers (Vwf, CD31, VE-Cadherin) were lower, whereas mRNA and protein levels of mesenchymal markers (Vimentin, α-SMA, Sm22α) were higher in *Pde4b*-overexpressed PAECs compared to control PAECs (Fig. 5J−N, Fig. S8J−S8R). These results further suggest that *Pde4b* promotes hypoxia-induced EndMT in PAECs.

After EndMT, ECs gain proliferative capacity and the ability to migrate, and these factors contribute to vascular remodeling[33,34]. We therefore assessed cell proliferation and migration in PAECs. We found that hypoxia-induced PAEC proliferation, as assessed by PCNA immunoblot analysis, CCK8 assay, and EdU labeling assay, was reduced by *Pde4b* knockdown (Supporting Information Fig. S9A−S9D). Moreover, in scratch wound and Transwell migration assays, hypoxia-induced PAEC migration was effectively attenuated by *Pde4b* knockdown (Fig. S9E−S9H).

3.7. PDE4B promotes PAEC EndMT via the PKA−CREB−BMPRII axis

PDE4 family members hydrolyze cAMP only, and the canonical cAMP effector molecules include cAMP-dependent PKA and exchange protein directly activated by cAMP (Epac)[35]. We thus investigated the effects of PKA- or Epac-specific inhibitors on PDE4B-mediated regulation of EndMT in PAECs. We found that culturing cells with a PKA inhibitor, PKI, rescued the *Pde4b*-knockdown phenotype (Fig. 6A−E), but the Epac inhibitor, ESI-09, did not change the effect of *Pde4b* knockdown on EndMT markers (Supporting Information Fig. S10A−S10E).

It is known that cAMP response element-binding protein (CREB), a downstream target of the cAMP−PKA pathway, can be activated by hypoxia[36]. To examine whether PDE4B regulates EndMT through CREB signaling, we transfected PAECs with *Creb* siRNA (Fig. S10F) or *Pde4b* siRNA or both *Creb* and *Pde4b* siRNA, which showed that *Creb* knockdown prevented the *Pde4b*-knockdown-induced inhibition of hypoxia-induced EndMT (Fig. 6F−J).

The critical role of bone morphogenetic protein receptor II (BMPRII) in PH has been demonstrated in numerous clinical and experimental studies. *Bmpr2* deficiency promotes EndMT and PH in mice[37], and, interestingly, BMPRII expression has been shown to be increased by stimulating the cAMP/PKA/CREB signaling pathway in osteoblasts[38]. Thus, we examined whether PDE4B promotes EndMT by antagonizing cAMP/PKA/CREB signaling and subsequently downregulating BMPRII in PAECs. As anticipated, we found that *Pde4b* knockdown increased BMPRII expression in hypoxic PAECs, and that the effect of *Pde4b* knockdown on BMPRII expression was blocked by a PKA inhibitor (Fig. 6K−M). In addition, the effect of *Pde4b* knockdown to increase BMPRII expression was also blocked by genetic *Creb* knockdown (Fig. 6N−P). In sum, these findings suggest that PDE4B promotes EndMT of PAECs by antagonizing the cAMP−PKA−CREB−BMPRII signaling axis.

3.8. PDE4B-specific inhibitor ameliorates the SuHx-induced rat PH phenotype

Since we found that the PDE4B isozyme among the PDE4 family plays a major role in PH development, specific inhibition of PDE4B is an ideal therapeutic strategy for treating PH while avoiding side effects caused by PDE4D inhibition. Recently, a new PDE4B-specific inhibitor (BI 1015550) has been developed and tested in phase III clinical trials[39,40]. We thus explored the therapeutic effect of BI 1015550 (the synthesis proceeded as published in a United States patent US8609670B2) in a rat PH model. SD rats at 6 weeks of age were injected with SU 5416 and placed under hypoxia (10% O_2) for 3 weeks, followed by two weeks under normoxic conditions (21% O_2) to establish PH. Subsequently, rats were randomly assigned to receive either the BI 1015550 (3.24 mg/kg·day, dissolved in 0.5% hydroxyethyl cellulose solution) or vehicle treatment *via* drinking water for an additional 2 weeks (Fig. 7A). The dose of BI 1015550 was determined from the dose used for treating human idiopathic pulmonary fibrosis[39] based on body surface area. We found that RVSP was reduced in the PH rats treated with BI 1015550 compared with the PH rats treated with vehicle (Fig. 7B). BI 1015550 treatment also significantly decreased the ratio of RV/(LV + S) (Fig. 7C) and improved PA AT/ET ratio (Fig. 7D). The average medial wall of distal pulmonary arteries was lower in PH rats treated with BI 1015550 than in PH rats treated with vehicle (Fig. 7E−H). Our findings indicate that BI 1015550 has a significant therapeutic effect in rat PH, and suggest that the PDE4-sepecific inhibitor may represent a novel and supreme therapeutic agent for PH compared to the pan-PDE4 inhibitor such as

subjected to Nox or SuHx. (I)−(N) Quantification of Vwf (I), CD31 (J), VE-Cadherin (K), Vimentin (L), α-SMA (M) and Sm22α (N) protein expression in (H) normalized to β-actin (fold change *versus* control). (O) Construction of the EC lineage tracing *Pde4b*$^{EC-/-}$/mTomato/mGFP-floxed dual-fluorescent Cre reporter (mTmG) mice. (P) Representative immunofluorescence staining of GFP and α-SMA in lung tissues of Tek Cre/mTmG or *Pde4b*$^{EC-/-}$/mTmG mice subjected to Nox or SuHx; scale bar = 50 μm. Similar results were obtained from at least 3 independent experiments. Data are expressed as mean ± SEM. For (B)−(G), (I)−(K), (N), the differences between groups were determined using two-way ANOVA followed by the Holm-Sidak's *post hoc* test. For (L) and (M), the differences between groups were determined using parametric Welch ANOVA with Dunnett's T3 *post hoc* test. *$P < 0.05$, **$P < 0.01$, ***$P < 0.001$, ****$P < 0.0001$.

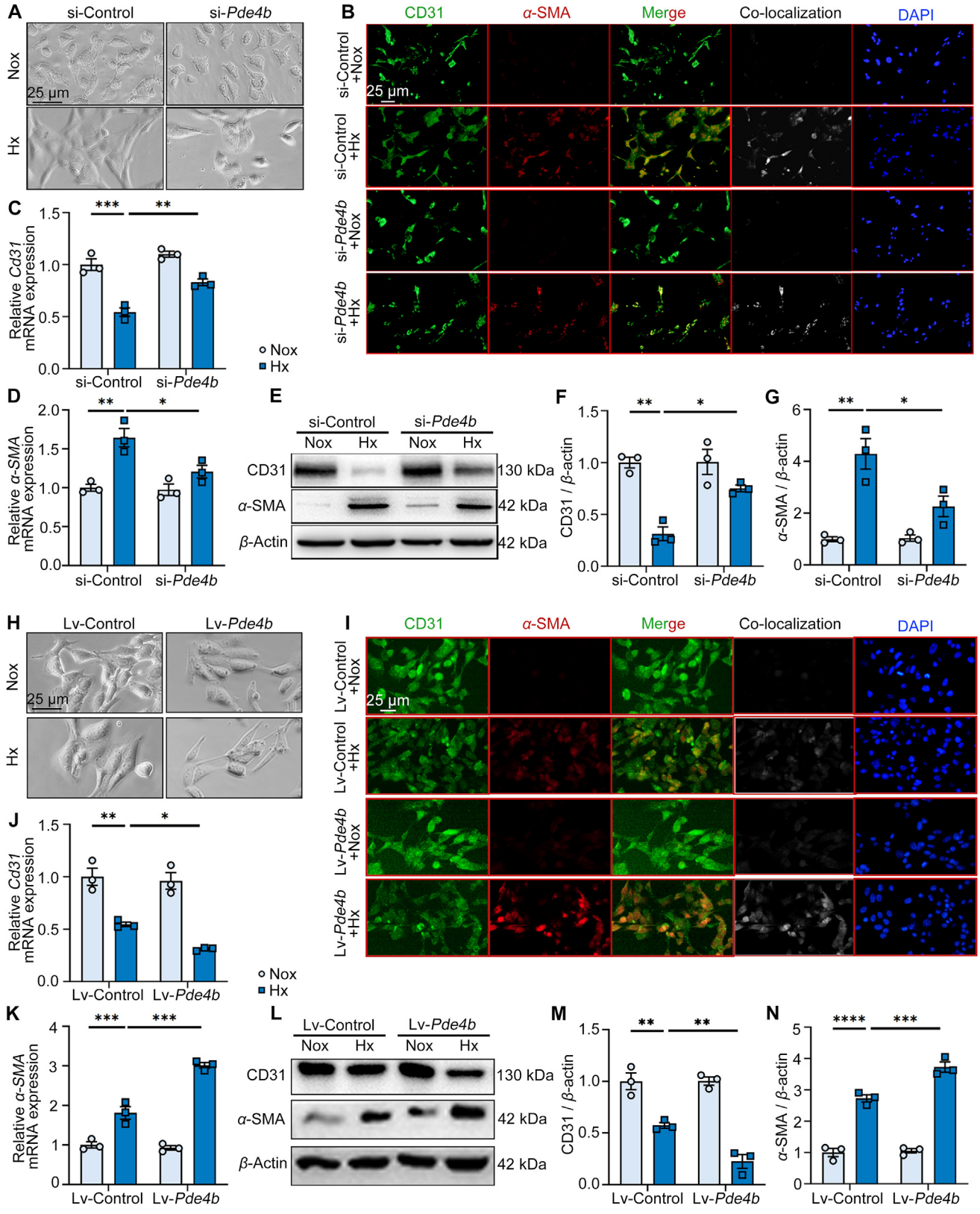

Figure 5 PDE4B promotes hypoxia-induced EndMT in mouse PAECs. (A) and (B) Representative micrographs (A) and immunostaining of CD31 and α-SMA (B) of PAECs exposed to hypoxia (Hx) and transfected with *Pde4b*-targeting siRNA or scramble control. Similar results were obtained from at least 3 independent experiments; scale bar = 25 μm. (C) and (D) RT-PCR analysis of *Cd31* (C), *α-SMA* (D) mRNA expression under indicated conditions. (E) Representative immunoblot analysis of CD31 and α-SMA under indicated conditions. (F)−(G) Quantification of CD31 (F) α-SMA (G) protein expression in (E) normalized to β-actin (fold change *versus* control). (H) Representative micrographs of PAECs

roflumilast with severe gastrointestinal side effects due to PDE4D inhibition.

4. Discussion

In this study, we identified PDE4B as the predominant PDE4 isoform contributing to PH development. Specifically, we illustrated that mRNA and protein levels of PDE4B were upregulated in the lung tissues of mouse, rat, and human with PH, and that the efficacy of the pan-PDE4 inhibitor, roflumilast, to alleviate PH in mice was primarily dependent on its inhibition of PDE4B. We further showed that PDE4B expression in ECs promotes EndMT during PH development by antagonizing the cAMP/PKA/CREB/BMPRII signaling pathway. Finally, we demonstrated that inhibiting PDE4B selectively using PDE4B-specific inhibitor (BI 1015550) can also significantly ameliorate PH in rats. The significance of our findings is highlighted by the fact that the PDE4B-specific inhibitor is entering phase III clinical trials for idiopathic pulmonary fibrosis. Thus, PDE4B-specific inhibition in human PH warrants further investigations.

Roflumilast is currently used in the clinical treatment of COPD owing to its inhibitory effect on airway inflammation[41]. A few studies have also reported that roflumilast improved MCT-induced PH in rats by inhibiting SMC proliferation and inflammation[14,15]. However, the specific PDE4 isozyme(s) responsible for the effect of roflumilast on PH were not defined in these previous studies. Our current study examines various genetically engineered rodent models to demonstrate a major role for PDE4B expressed in ECs in PH development and show that the roflumilast-mediated improvements in PH result from its inhibition of PDE4B. Roflumilast is associated with side effects that can limit patient compliance, including gastrointestinal side effects such as nausea and vomiting, and previous studies showed that PDE4D expressed in the area postrema and nucleus of the solitary tract is responsible for emetic symptoms[16,17]. Also, *Pde4d*^{KO} mice are resistant to xylazine/ketamine-induced anesthesia, a behavior correlated with emesis in rodents[42]. Thus, a more specific strategy targeting of PDE4B may alleviate PH while avoiding adverse reactions associated with PDE4D inhibition.

ECs play an important role during PH development[43], as damaged ECs secrete inflammatory factors and cytokines, and may undergo apoptosis, phenotypic transformation, proliferation, and migration. The functions of medium SMCs and outer membrane fibroblasts may also be altered[44]. Interestingly, the contribution of EndMT to PH development is still controversial. For example, using EC lineage tracing mice, Qiao et al.[45] reported the expression of mesenchymal cell markers, proliferation, and migration of EC-originated SMC-like cells during PH development, thus supporting a role for EndMT in PH. In contrast, a recent study using both SMC-lineage-tracing and EC-lineage-tracing mice did not find evidence of EndMT during PH development[46]. The discrepancy between these two studies may be owing to differences in mouse strains and/or models of PH. In the former study, PH was induced in C57BL/6 J mice by a left pneumonectomy combined with monocrotaline pyrrole. In the latter study, PH was induced in BALB/c mice by house dust mite combined with hypoxia and SuHx. In our study, PH was induced by SuHx in C57BL/6 J mice with EC lineage tracing, and our results confirm that EndMT contributes to the pathogenesis of PH, specifically identifying a role for PDE4B expression in ECs to promote EndMT and vascular remodeling. In addition, our *in vitro* studies demonstrated the ability of PAECs to transform into mesenchymal cells, as well as to proliferate and migrate, and that the development of these phenotypes were PDE4B dependent. Further studies are required to clarify the contribution of EndMT to PH with different etiologies.

In human and rodent lung PH tissues, we found that PDE4B upregulation primarily occurred in ECs. To determine the role of PDE4B expression in ECs in PH, we compared the effects of global *Pde4b* and EC-specific *Pde4b* knockout on EndMT and on PH development. Interestingly, both conditions resulted in very similar protective effects against EndMT and PH, suggesting EC-specific PDE4B may play a dominant role in disease development. Although our results primarily point to PDE4B expression in ECs as the driver of PH in the models studied, we do not exclude contributions of other PDE4 isozymes in other cell types[47] and the possibility that PDE4B may also regulate the EC-secreted factors (such as PDGFB[48,49], CXCL12[50], FGF2[51], and endothelin-1[52]) that subsequently promote SMC proliferation. SMC proliferation and immune cell-mediated inflammation have been well documented in PH[44]. For example, pan-PDE4 inhibitors elicited anti-proliferative effects in human pulmonary artery smooth muscle cells (PASMCs)[53], and they also reduced interleukin-6 and monocyte chemotactic protein-1 mRNA levels in MCT-induced PH lung tissues[14]. The precise roles of specific PDE4 isozyme(s) in SMCs and inflammatory cells during PH development warrant further investigation.

The clinical trials with PDE4B-selective inhibitor BI 1015550 in treating idiopathic pulmonary fibrosis (IPF) have made promising progress[39]. Mechanistically, BI 1015550 was found to inhibit the LPS-induced release of inflammatory cytokines, such as TNF-α and IL-2, by mononuclear cells in peripheral blood and to inhibit macrophage and neutrophil influx into the bronchoalveolar[40]. Since the uncontrolled activation of fibroblasts and extracellular matrix deposition in lung fibrosis are associated with the involvement of inflammatory cells and cytokines, the effect of BI 1015550 on IPF is mainly through suppressing inflammation[54]. In the current study, we demonstrated a significant effect of BI 1015550 on treating PH in pre-clinical animal models. We focused on the role of PDE4B in EC EndMT and the subsequent myofibroblast proliferation and migration. In addition, the role of PDE4B in SMC proliferation may also be one of the pharmacological mechanisms of BI 1015550[47]. These results suggest that BI 1015550 may treat IPF and PH through different mechanisms. However, the proinflammatory function of PDE4B may also contribute to pulmonary vascular remodeling in PH, which needs further investigation.

exposed to Hx and/or *Pde4b*-expressing lentiviral vectors (Lv-*Pde4b*); scale bar = 25 μm. Similar results were obtained from at least 3 independent experiments. (I) Representative immunofluorescence staining of CD31 and α-SMA in PAECs exposed to Hx and/or Lv-*Pde4b*; scale bar = 25 μm. Similar results were obtained from at least 3 independent experiments. (J)−(K) RT-PCR analysis of *Cd31* (J) *α-SMA* (K) mRNA expression under indicated conditions. (L) Representative immunoblot analysis of CD31 and α-SMA under indicated conditions. (M)−(N) Quantification of CD31 (M) α-SMA (N) protein expression in (L) normalized to β-actin (fold change *versus* control). $n = 3$ independent experiments. Data are expressed as mean ± SEM. For (C), (D), (F), (G), (J), (K), (M), (N), the differences between groups were determined using two-way ANOVA followed by the Holm-Sidak's *post hoc* test. $^{*}P < 0.05$, $^{**}P < 0.01$, $^{***}P < 0.001$, $^{****}P < 0.0001$.

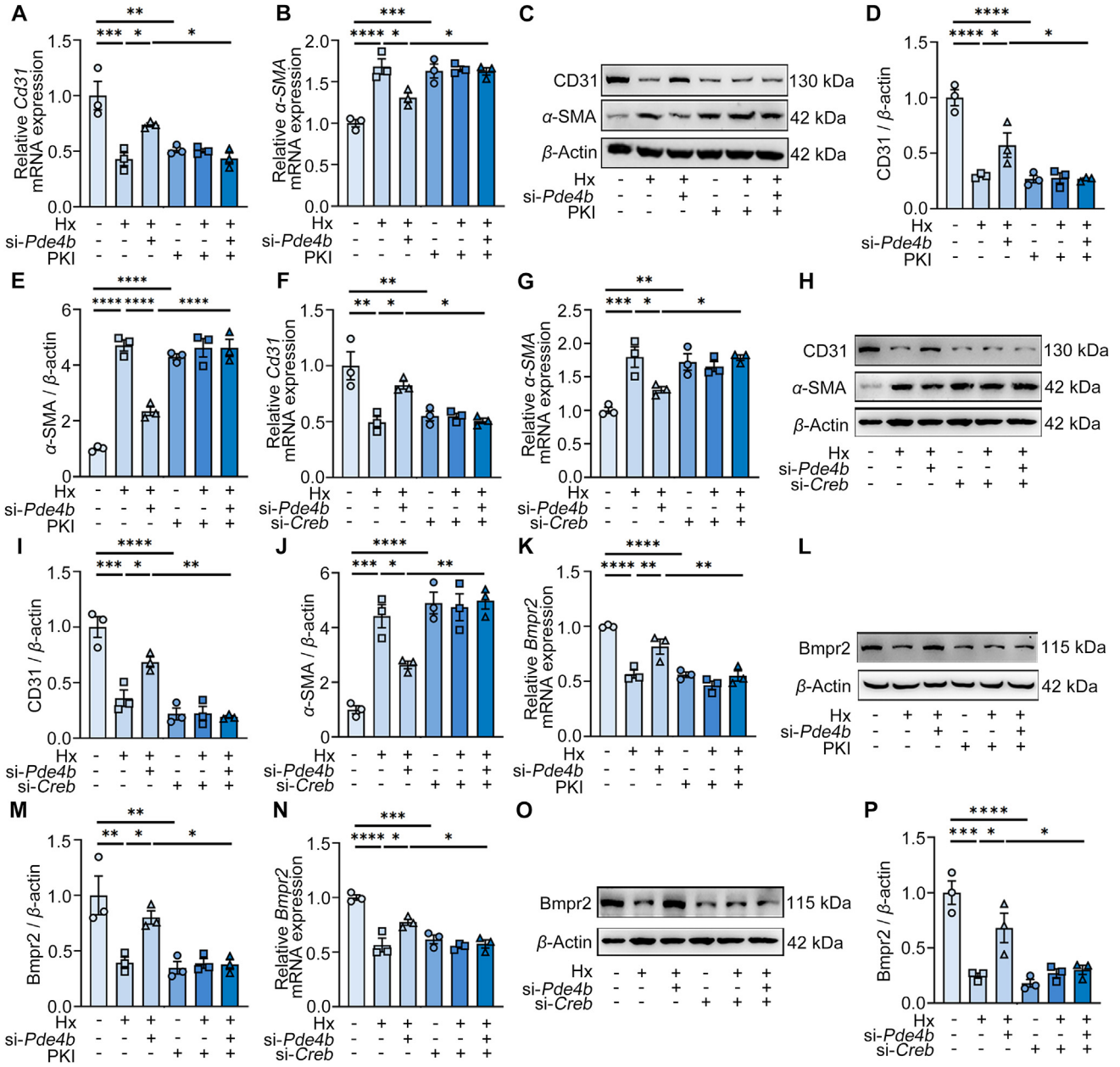

Figure 6 PDE4B promotes EndMT by attenuating the PKA−CREB−BMPRII axis. (A, B) RT-PCR analysis of *Cd31* (A) and *α-SMA* (B) mRNA expression under indicated conditions. (C) Representative immunoblot analysis of CD31 and α-SMA in PAECs exposed to hypoxia (Hx) transfected with *Pde4b* siRNA or scramble control and with or without PKI, as indicated. (D, E) Quantification of CD31 (D) and α-SMA (E) protein expression in (C) normalized to β-actin (fold change *versus* control). (F, G) RT-PCR analysis of *Cd31* (F) and *α-SMA* (G) mRNA expression under indicated conditions. (H) Representative immunoblot analysis of CD31 and α-SMA in PAECs exposed to Hx and/or si-*Pde4b* or si-Control and/or si-*Creb* or si-Control, as indicated. (I, J) Quantification of CD31 (I) and α-SMA (J) protein expression in (H) normalized to β-actin (fold change *versus* control). (K) RT-PCR analysis of *Bmpr2* mRNA expression under indicated conditions. (L) Representative immunoblot analysis of BMPRII in PAECs as indicated. (M) Quantification of BMPRII protein expression in (l) normalized to β-actin (fold change *versus* control). (N) RT-PCR analysis of *Bmpr2* mRNA expression under indicated conditions. (O) Representative immunoblot analysis of BMPRII in PAECs treated as indicated in (H). (P) Quantification of BMPRII protein expression in (O) normalized to β-actin (fold change *versus* control). Data are expressed as mean ± SEM. For (A), (B), (D)−(G), (I)−(K), (M), (N), (P), the differences between groups were determined using parametric one-way ANOVA followed by the Holm-Sidak's *post hoc* test. *$P < 0.05$, **$P < 0.01$, ***$P < 0.001$, ****$P < 0.0001$.

PDE5 inhibitors, such as sildenafil and tadalafil, are approved for the treatment of PH[55,56]. The PDE5A isozyme in the pulmonary arterial SMCs causes pulmonary artery constriction by specific hydrolysis of cGMP, an important second messenger in vascular relaxation[8]. Thus, PDE5 inhibition elicits a beneficial effect on hemodynamics, which improves pulmonary artery vasoconstriction, RV hypertrophy, and cardiovascular function[57]. In this study, we reported a critical role of a different PDE

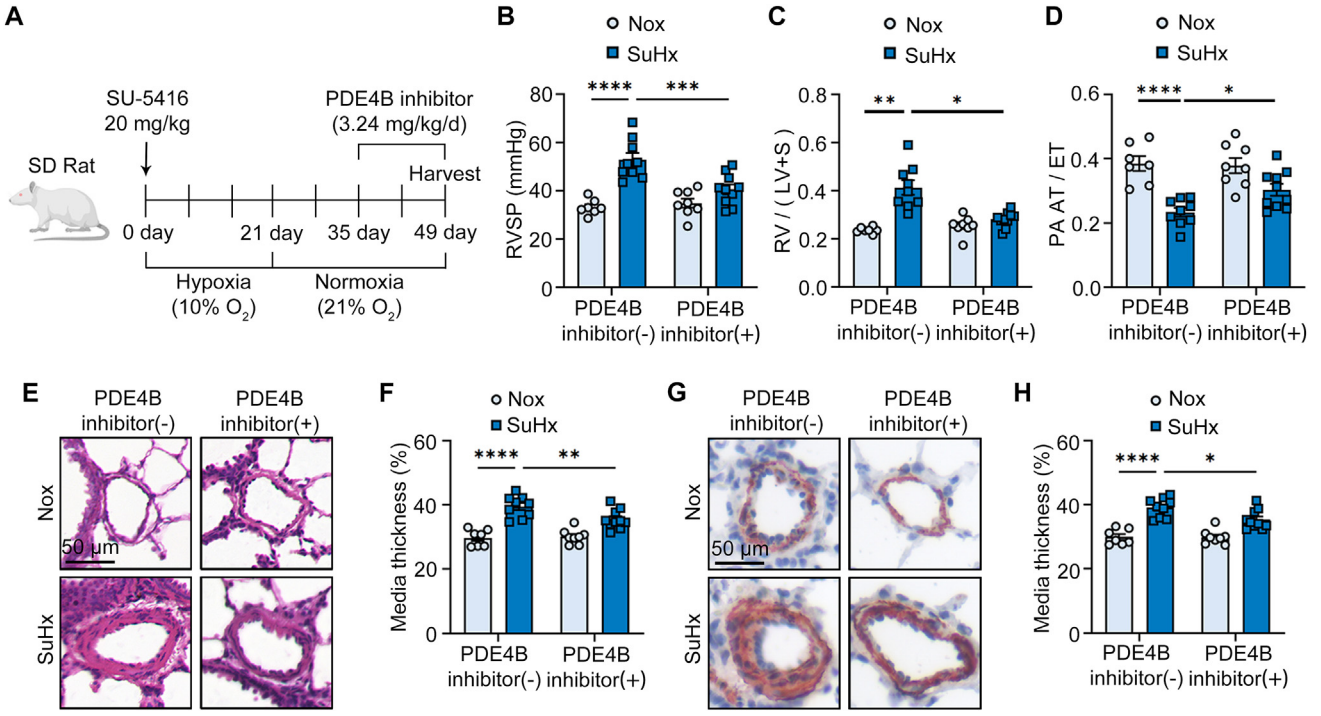

Figure 7 PDE4B-specific inhibitor ameliorates the SuHx-induced rat PH phenotype. (A) SD rats subjected to Nox or SuHx were treated with vehicle or PDE4B inhibitor *via* drinking water for 2 weeks. Healthy rats treated with vehicle ($n = 7$) or PDE4B inhibitor ($n = 8$); PH rats treated with vehicle ($n = 9$) or PDE4B inhibitor ($n = 10$). (B)−(D) RVSP (B), ratio of RV/(LV + S) (C), cardiac echo analysis of PA AT/ET ratio (D) of indicated groups of rats in (A). (E) Representative H&E staining images of pulmonary arteries under the indicated experimental conditions; scale bar = 50 μm. (F) Pulmonary arterial wall thickness of rats in (E). (G) Representative immunostaining of α-SMA in lung tissues under the indicated experimental conditions; scale bar = 50 μm. (H) Pulmonary arterial wall thickness of rats in (G). Data are expressed as mean ± SEM. For (B), (D), (F), (H), the differences between groups were determined using two-way ANOVA followed by the Holm-Sidak's *post hoc* test. For (C), the differences between groups were determined using parametric Welch ANOVA with Dunnett's T3 *post hoc* test. $^{*}P < 0.05$, $^{**}P < 0.01$, $^{***}P < 0.001$, $^{****}P < 0.0001$.

member, PDE4B, in PH and show that PDE4B contributes to PH primarily by inducing EndMT and arterial structure remodeling *via* inhibition of the cAMP/PKA/CREB-dependent regulation of BMPRII. Given the distinct mechanistic actions of PDE4B and PDE5A in PH, whether combined PDE4B and PDE5A inhibition may have additive or synergistic effects to alleviate PH is an interesting question for future research. Indeed, a previous study showed that a small molecule compound inhibiting both PDE4 and PDE5 improved PH and pulmonary vascular remodeling more effectively than the PDE5 inhibitor sildenafil alone[58], but it is expected that using more specific inhibitors of PDE4B and PDE5A would be associated with fewer side effects.

5. Conclusions

Taken together, our data support a model in which elevated PDE4B expression in ECs inhibits the PKA−CREB−BMPRII axis, increases EndMT, and promotes SuHx-induced PH development. Our findings strongly suggest that PDE4B is a novel therapeutic target for PH treatment.

Acknowledgments

This work was supported by Beijing Natural Science Foundation [Z220019 to Jing Wang, China]; National High Level of Hospital Clinical Research Funding [2022-PUMCH-D-002 to Jing Wang, China]; National Key Research and Development Program of China Grants [2019YFA0801703 and 2019YFA0801804 to Jing Wang]; Chinese Academy of Medical Sciences Innovation Fund for Medical Sciences [2022-I2M-JB-007 to Chen Wang, 2021-I2M-1-016 to Hongmei Zhao, 2021-I2M-1-049 to Jing Wang, 2021-I2M-1-005 to Yanjiang Xing, China]; Haihe Laboratory of Cell Ecosystem Innovation Fund [22HHXBSS00010 to Jing Wang, China]; National Natural Science Foundation of China [82241004 to Jing Wang].

Author contributions

Yanjiang Xing, Yangfeng Hou, Tianfei Fan, and Ran Gao wrote the manuscript and prepared the figures. Yanjiang Xing, Yangfeng Hou, Tianfei Fan, Ran Gao, Xiaohang Feng, Wenjun Guo, Ting Shu, Jinqiu Li, Jie Yang, Qilong Mao, Ya Luo, and Xianmei Qi performed the animal experiments. Yanjiang Xing, Yangfeng Hou, Tianfei Fan, Ran Gao, and Xiaohang Feng performed the cell experiments. Junling Pang, Bolun Li performed the data analysis. Peiran Yang revised the language of the manuscript. Chaoyang Liang and Wenhui Chen provided human samples. Yanjiang Xing, Peiran Yang, Hongmei Zhao, Wenhui Chen, and Jing Wang designed the research. Jing Wang and Chen Wang provided financial support.

Conflicts of interest

The authors declare no conflicts of interest.

Appendix A. Supporting information

Supporting data to this article can be found online at https://doi.org/10.1016/j.apsb.2024.01.012.

References

1. Rich S, Haworth SG, Hassoun PM, Yacoub MH. Pulmonary hypertension: the unaddressed global health burden. *Lancet Respir Med* 2018;**6**:577−9.
2. Sadek MS, Cachorro E, El-Armouche A, Kämmerer S. Therapeutic implications for PDE2 and cGMP/cAMP mediated crosstalk in cardiovascular diseases. *Int J Mol Sci* 2020;**21**:7462.
3. Bubb KJ, Trinder SL, Baliga RS, Patel J, Clapp LH, MacAllister RJ, et al. Inhibition of phosphodiesterase 2 augments cGMP and cAMP signaling to ameliorate pulmonary hypertension. *Circulation* 2014;**130**:496−507.
4. Kumar N, Goldminz AM, Kim N, Gottlieb AB. Phosphodiesterase 4-targeted treatments for autoimmune diseases. *BMC Med* 2013;**11**:96.
5. Chen S, Yan C. An update of cyclic nucleotide phosphodiesterase as a target for cardiac diseases. *Expet Opin Drug Discov* 2021;**16**:183−96.
6. Santos-Silva AJ, Cairrao E, Morgado M, Alvarez E, Verde I. PDE4 and PDE5 regulate cyclic nucleotides relaxing effects in human umbilical arteries. *Eur J Pharmacol* 2008;**582**:102−9.
7. Patel BS, Prabhala P, Oliver BG, Ammit AJ. Inhibitors of phosphodiesterase 4, but not phosphodiesterase 3, increase β2-agonist-induced expression of antiinflammatory mitogen-activated protein kinase phosphatase 1 in airway smooth muscle cells. *Am J Respir Cell Mol Biol* 2015;**52**:634−40.
8. Corbin JD, Beasley A, Blount MA, Francis SH. High lung PDE5: a strong basis for treating pulmonary hypertension with PDE5 inhibitors. *Biochem Biophys Res Commun* 2005;**334**:930−8.
9. Li H, Zuo J, Tang W. Phosphodiesterase-4 inhibitors for the treatment of inflammatory diseases. *Front Pharmacol* 2018;**9**:1048.
10. Barnes PJ. Cyclic nucleotides and phosphodiesterases and airway function. *Eur Respir J* 1995;**8**:457−62.
11. Torphy TJ. Phosphodiesterase isozymes: molecular targets for novel antiasthma agents. *Am J Respir Crit Care Med* 1998;**157**:351−70.
12. Zebda R, Paller AS. Phosphodiesterase 4 inhibitors. *J Am Acad Dermatol* 2018;**78**:S43−52.
13. Facchinetti F, Civelli M, Singh D, Papi A, Emirova A, Govoni M. Tanimilast, a novel inhaled PDE4 inhibitor for the treatment of asthma and chronic obstructive pulmonary disease. *Front Pharmacol* 2021;**12**:740803.
14. Izikki M, Raffestin B, Klar J, Hatzelmann A, Marx D, Tenor H, et al. Effects of roflumilast, a phosphodiesterase-4 inhibitor, on hypoxia- and monocrotaline-induced pulmonary hypertension in rats. *J Pharmacol Exp Therapeut* 2009;**330**:54−62.
15. Nose T, Kondo M, Shimizu M, Hamura H, Yamaguchi Y, Sekine T, et al. Pharmacological profile of GPD-1116, an inhibitor of phosphodiesterase 4. *Biol Pharm Bull* 2016;**39**:689−98.
16. Xing M, Akowuah GA, Gautam V, Gaurav A. Structure-based design of selective phosphodiesterase 4B inhibitors based on ginger phenolic compounds. *J Biomol Struct Dyn* 2017;**35**:2910−24.
17. Al-Nema M, Gaurav A, Lee VS. Docking based screening and molecular dynamics simulations to identify potential selective PDE4B inhibitor. *Heliyon* 2020;**6**:e04856.
18. Galie N, Humbert M, Vachiery JL, Gibbs S, Lang I, Torbicki A, et al. ESC/ERS guidelines for the diagnosis and treatment of pulmonary hypertension: the joint task force for the diagnosis and treatment of pulmonary hypertension of the European society of cardiology (ESC) and the European respiratory society (ERS): endorsed by: association for European paediatric and congenital cardiology (AEPC), international society for heart and lung transplantation (ISHLT). *Eur Heart J* 2015;**2016**(37):67−119.
19. Oakes JM, Xu J, Morris TM, Fried ND, Pearson CS, Lobell TD, et al. Effects of chronic nicotine inhalation on systemic and pulmonary blood pressure and right ventricular remodeling in mice. *Hypertension* 2020;**75**:1305−14.
20. Dai Z, Zhu MM, Peng Y, Machireddy N, Evans CE, Machado R, et al. Therapeutic targeting of vascular remodeling and right heart failure in pulmonary arterial hypertension with a HIF-2alpha inhibitor. *Am J Respir Crit Care Med* 2018;**198**:1423−34.
21. Zhao Y, Wang B, Zhang J, He D, Zhang Q, Pan C, et al. ALDH2 (aldehyde dehydrogenase 2) protects against hypoxia-induced pulmonary hypertension. *Arterioscler Thromb Vasc Biol* 2019;**39**:2303−19.
22. Suen CM, Chaudhary KR, Deng Y, Jiang B, Stewart DJ. Fischer rats exhibit maladaptive structural and molecular right ventricular remodelling in severe pulmonary hypertension: a genetically prone model for right heart failure. *Cardiovasc Res* 2019;**115**:788−99.
23. Chen Y, Kuang M, Liu S, Hou C, Duan X, Yang K, et al. A novel rat model of pulmonary hypertension induced by mono treatment with SU5416. *Hypertens Res* 2020;**43**:754−64.
24. Li P, Xing J, Zhang J, Jiang J, Liu X, Zhao D, et al. Inhibition of long noncoding RNA HIF1A-AS2 confers protection against atherosclerosis *via* ATF2 downregulation. *J Adv Res* 2020;**26**:123−35.
25. Wang W, Zhang S, Xu L, Feng Y, Wu X, Zhang M, et al. Involvement of circHIPK3 in the pathogenesis of diabetic cardiomyopathy in mice. *Diabetologia* 2021;**64**:681−92.
26. Hu Y, Rao SS, Wang ZX, Cao J, Tan YJ, Luo J, et al. Exosomes from human umbilical cord blood accelerate cutaneous wound healing through miR-21-3p-mediated promotion of angiogenesis and fibroblast function. *Theranostics* 2018;**8**:169−84.
27. Carter K, Lee HJ, Na KS, Fernandes-Cunha GM, Blanco IJ, Djalilian A, et al. Characterizing the impact of 2D and 3D culture conditions on the therapeutic effects of human mesenchymal stem cell secretome on corneal wound healing *in vitro* and *ex vivo*. *Acta Biomater* 2019;**99**:247−57.
28. Liu Z, Wang Y, Dou C, Xu M, Sun L, Wang L, et al. Hypoxia-induced up-regulation of VASP promotes invasiveness and metastasis of hepatocellular carcinoma. *Theranostics* 2018;**8**:4649−63.
29. Taraseviciene-Stewart L, Kasahara Y, Alger L, Hirth P, Mc Mahon G, Waltenberger J, et al. Inhibition of the VEGF receptor 2 combined with chronic hypoxia causes cell death-dependent pulmonary endothelial cell proliferation and severe pulmonary hypertension. *Faseb J* 2001;**15**:427−38.
30. Arciniegas E, Frid MG, Douglas IS, Stenmark KR. Perspectives on endothelial-to-mesenchymal transition: potential contribution to vascular remodeling in chronic pulmonary hypertension. *Am J Physiol Lung Cell Mol Physiol* 2007;**293**:L1−8.
31. Ranchoux B, Antigny F, Rucker-Martin C, Hautefort A, Péchoux C, Bogaard HJ, et al. Endothelial-to-mesenchymal transition in pulmonary hypertension. *Circulation* 2015;**131**:1006−18.
32. Diez M, Musri MM, Ferrer E, Barbera JA, Peinado VI. Endothelial progenitor cells undergo an endothelial-to-mesenchymal transition-like process mediated by TGFbetaRI. *Cardiovasc Res* 2010;**88**:502−11.
33. Welch-Reardon KM, Wu N, Hughes CC. A role for partial endothelial-mesenchymal transitions in angiogenesis?. *Arterioscler Thromb Vasc Biol* 2015;**35**:303−8.
34. Sakao S, Tatsumi K, Voelkel NF. Endothelial cells and pulmonary arterial hypertension: apoptosis, proliferation, interaction and transdifferentiation. *Respir Res* 2009;**10**:95.
35. Cheng X, Ji Z, Tsalkova T, Mei F. Epac and PKA: a tale of two intracellular cAMP receptors. *Acta Biochim Biophys Sin* 2008;**40**:651−62.
36. Leonard MO, Howell K, Madden SF, Costello CM, Higgins DG, Taylor CT, et al. Hypoxia selectively activates the CREB family of transcription factors in the *in vivo* lung. *Am J Respir Crit Care Med* 2008;**178**:977−83.
37. Hopper RK, Moonen JR, Diebold I, Cao A, Rhodes CJ, Tojais NF, et al. In pulmonary arterial hypertension, reduced BMPR2 promotes endothelial-to-mesenchymal transition *via* HMGA1 and its target slug. *Circulation* 2016;**133**:1783−94.

38. Zhou W, Yu L, Fan J, Wan B, Jiang T, Yin J, et al. Endogenous parathyroid hormone promotes fracture healing by increasing expression of BMPR2 through cAMP/PKA/CREB pathway in mice. *Cell Physiol Biochem* 2017;**42**:551−63.
39. Richeldi L, Azuma A, Cottin V, Hesslinger C, Stowasser S, Valenzuela C, et al. Trial of a preferential phosphodiesterase 4B inhibitor for idiopathic pulmonary fibrosis. *N Engl J Med* 2022;**386**:2178−87.
40. Herrmann FE, Hesslinger C, Wollin L, Nickolaus P. BI 1015550 is a PDE4B inhibitor and a clinical drug candidate for the oral treatment of idiopathic pulmonary fibrosis. *Front Pharmacol* 2022;**13**:838449.
41. Kawamatawong T. Roles of roflumilast, a selective phosphodiesterase 4 inhibitor, in airway diseases. *J Thorac Dis* 2017;**9**:1144−54.
42. Robichaud A, Stamatiou PB, Jin SL, Lachance N, MacDonald D, Laliberté F, et al. Deletion of phosphodiesterase 4D in mice shortens α_2-adrenoceptor-mediated anesthesia, a behavioral correlate of emesis. *J Clin Invest* 2002;**110**:1045−52.
43. Evans CE, Cober ND, Dai Z, Stewart DJ, Zhao YY. Endothelial cells in the pathogenesis of pulmonary arterial hypertension. *Eur Respir J* 2021;**58**:2003957.
44. Thenappan T, Ormiston ML, Ryan JJ, Archer SL. Pulmonary arterial hypertension: pathogenesis and clinical management. *BMJ* 2018;**360**:j5492.
45. Qiao L, Nishimura T, Shi L, Sessions D, Thrasher A, Trudell JR, et al. Endothelial fate mapping in mice with pulmonary hypertension. *Circulation* 2014;**129**:692−703.
46. Steffes LC, Froistad AA, Andruska A, Boehm M, McGlynn M, Zhang F, et al. A Notch3-marked subpopulation of vascular smooth muscle cells is the cell of origin for occlusive pulmonary vascular lesions. *Circulation* 2020;**142**:1545−61.
47. Pan Z, Wu X, Zhang X, Hu K. Phosphodiesterase 4B activation exacerbates pulmonary hypertension induced by intermittent hypoxia by regulating mitochondrial injury and cAMP/PKA/p-CREB/PGC-1α signaling. *Biomed Pharmacother* 2023;**158**:114095.
48. Guignabert C, Alvira CM, Alastalo TP, Sawada H, Hansmann G, Zhao M, et al. Tie2-mediated loss of peroxisome proliferator-activated receptor-gamma in mice causes PDGF receptor-beta-dependent pulmonary arterial muscularization. *Am J Physiol Lung Cell Mol Physiol* 2009;**297**:L1082−90.
49. ten Freyhaus H, Dagnell M, Leuchs M, Vantler M, Berghausen EM, Caglayan E, et al. Hypoxia enhances platelet-derived growth factor signaling in the pulmonary vasculature by down-regulation of protein tyrosine phosphatases. *Am J Respir Crit Care Med* 2011;**183**:1092−102.
50. Dai Z, Li M, Wharton J, Zhu MM, Zhao YY. Prolyl-4 hydroxylase 2 (PHD2) deficiency in endothelial cells and hematopoietic cells induces obliterative vascular remodeling and severe pulmonary arterial hypertension in mice and humans through hypoxia-inducible factor-2α. *Circulation* 2016;**133**:2447−58.
51. Kim J, Kang Y, Kojima Y, Lighthouse JK, Hu X, Aldred MA, et al. An endothelial apelin-FGF link mediated by miR-424 and miR-503 is disrupted in pulmonary arterial hypertension. *Nat Med* 2013;**19**:74−82.
52. Yanagisawa M, Kurihara H, Kimura S, Tomobe Y, Kobayashi M, Mitsui Y, et al. A novel potent vasoconstrictor peptide produced by vascular endothelial cells. *Nature* 1988;**332**:411−5.
53. Growcott EJ, Spink KG, Ren X, Afzal S, Banner KH, Wharton J. Phosphodiesterase type 4 expression and anti-proliferative effects in human pulmonary artery smooth muscle cells. *Respir Res* 2006;**7**:9.
54. Sgalla G, Simonetti J, Cortese S, Richeldi L. BI 1015550: an investigational phosphodiesterase 4B (PDE4B) inhibitor for lung function decline in idiopathic pulmonary fibrosis (IPF). *Expet Opin Invest Drugs* 2023;**32**:17−23.
55. Galie N, Brundage BH, Ghofrani HA, Oudiz RJ, Simonneau G, Safdar Z, et al. Tadalafil therapy for pulmonary arterial hypertension. *Circulation* 2009;**119**:2894−903.
56. Galie N, Ghofrani HA, Torbicki A, Barst RJ, Rubin LJ, Badesch D, et al. Sildenafil citrate therapy for pulmonary arterial hypertension. *N Engl J Med* 2005;**353**:2148−57.
57. Fan YF, Zhang R, Jiang X, Wen L, Wu DC, Liu D, et al. The phosphodiesterase-5 inhibitor vardenafil reduces oxidative stress while reversing pulmonary arterial hypertension. *Cardiovasc Res* 2013;**99**:395−403.
58. Muraki Y, Naito T, Tohyama K, Shibata S, Kuniyeda K, Nio Y, et al. Improvement of pulmonary arterial hypertension, inflammatory response, and epithelium injury by dual activation of cAMP/cGMP pathway in a rat model of monocrotaline-induced pulmonary hypertension. *Biosci Biotechnol Biochem* 2019;**83**:1000−10.